Flexible Micro-Nano Fiber Sensors for Tactile Sensing

Wang, Yunkai; Jiang, Chunlei ; Dong, Taiji; Liu, Xu; Chen, Peng; yu, xianli; Yue, Liyang; Wang, Zengbo (James)

IEEE Sensors Journal

DOI:
10.1109/JSEN.2023.3344381

Published: 15/02/2024

Peer reviewed version

Flexible Micro-Nano Fiber Sensors for Tactile Sensing

Yunkai Wang[1], Chunlei Jiang[1,*], Taiji Dong[1], Xu Liu[1], Peng Chen[1], Xianli Yu[2], Liyang Yue[3], and Zengbo Wang[3,*]

[1] College of Electrical and Information Engineering, SANYA Offshore Oil and Gas Research Institute, Northeast Petroleum University, Daqing 163318, China

[2] College of Geo-Exploration Science and Technology, Jilin University, Changchun 130021, China

[3] School of Computer Science and Electronic Engineering, Bangor University, LL57 1UT Bangor, U.K.

*Corresponding authors: Chunlei Jiang (jiangchunlei_nepu@163.com); Zengbo Wang (z.wang@bangor.ac.uk)

Abstract—Flexible tactile sensors play an important role in wearable devices, human–computer interaction devices, and advanced robotics. We propose a novel structure of bionic flexible tactile sensor. The micro-nano fibers (MNFs) are packed in a 10-μm film on a polydimethylsiloxane (PDMS) base, forming a thin film-MNF-PDMS structure. A ridge shaped sensing region is formed on the surface of the PDMS substrate. The MNF is so close to the sensor surface that vibration and pressure signals can act directly on the MNF. Compared to existing MNF flexible sensors, this sensor has higher sensitivity and faster response time. We tested the response of the flexible sensor to vibration and temperature. This sensor can measure vibration signals from 0.1 Hz to 2 kHz. The sensitivity of this sensor to temperature can reach 1.43 nm/◦C. Surfaces with different roughness or texture can be distinguished by sliding on the sensor surface. The structural and functional characteristics of this sensor are desirable in flexible bionic devices and advanced robots.

Index Terms—Flexible sensors, micro-nano fiber (MNF), optical fiber sensor, tactile sensing.

I. INTRODUCTION

Tactile sensation, as an important human perception and collection function, has become a focus of research and development in recent years [1], [2]. The skin contains a variety of sensory nerves, such as low threshold mechanoreceptors (LTMRs) [3], which are sensitive to mechanical vibrations. When the skin touches an object, the LTMRs encode the perceived stress changes as well as the amplitude of the vibration into weak electrical signals that communicate with the nerve endings through protrusive transmission [4]. In recent years, emerging tactile sensing devices inspired by biological touch have mimicked the sensing

function of biological nerves. Tactile sensors that measure external mechanical forces, pressure, or vibration at a surface have been widely used in industrial [5], medical [6], and consumer applications [7].

In general, tactile sensors can be divided into two types according to the measurement principle, which are electrical-based [8], [9] and optical-based [10], [11], [12]. Electrical-based tactile sensors are designed to convert external mechanical vibrations into changes in voltage, current, capacitance, or resistance. Optical-based tactile sensors [13] can convert external mechanical vibrations into changes in beam intensity, phase, or wavelength. Relative to the current stateof-the-art bulk-based planar integrated-circuit sensor devices, flexible, bendable, and flexible sensor devices are compatible with curved, movable robot joints and human bodies [14]. With the development of nanotechnology and flexible electronics, flexible tactile sensors [15] have been able to achieve precise detection of physical changes such as pressure, temperature, and humidity.

Compared to electrical-based sensors, optical sensors, especially optical fiber sensors, have the advantages of antielectromagnetic interference, high sensitivity, fast response, and small size for multiparameter detection. To get closer to the function of biological neurogenic tactile sensing, it is important to have fiber optic sensors that can provide a richer and more natural form of feedback to external vibrations and stimuli.

Optical micro-nano fiber (MNF) [16], as a special optical fiber with a diameter close to or lower than visible or infrared light, has a wide range of applications for optical sensing at the micrometer and nanometer scales. Tactile sensors made from MNFS [10], [17] have a small footprint, high sensitivity, fast response, high flexibility, and low optical power. Micro and nanofiber optic sensors have also been studied a lot for tactile sensing. Recently, Yao et al. [18] solved the crosstalk of the optical signals of temperature and pressure by introducing different mechanisms of laser with different wavelengths conduction in MNFs. They realize the simultaneous measurement of temperature and pressure signals.

MNFs with a diameter of only a few micrometers can have large evanescent fields and optical confinement. Therefore, MNFs are susceptible to environmental stimuli. Weak pressure and vibration can cause changes in optical transmission and light intensity. Benefiting from the ultrasensitivity and enhanced evanescent fields of the MNF, the tactile sensors assembled with it have great potential for applications [19]. Compared to fiber Bragg grating (FBG) sensors [20], [21], which have become more popular in recent years, micronano optical fibers are simpler to manufacture, and the sensor structure can be more compact. Existing MNF-based sensors usually package the MNF in a flexible polydimethylsiloxane (PDMS) to manage the evanescent field and protect the MNF. However, there is still a lack of research on bioinspired or biomimetic optical sensors with object surface texture and roughness detection.

In this work, we propose a bionic flexible tactile sensor based on thin film-MNF-PDMS structure. We use a 10-μm film to cover the MNF on PDMS for packaging. A ridgeshaped sensing region is formed on the surface of the PDMS substrate. The MNF is so close to the sensor surface that vibration and pressure signals can act directly on the MNF. Such encapsulated MNF detects external stimuli in a manner similar to the sensory receptors and nerve fibers in the skin. Benefiting from these bionic structures and designs, photonic skin can effectively detect mechanical stimuli such as pressure and vibration in the form of changes in the intensity of transmitted light output. We tested the sensor's response to vibration, contact surface roughness, and temperature. The structural and functional characteristics of this sensor are desirable in flexible bionic devices and advanced robots.

II. METHODS AND PRINCIPLES

A. Materials and Methods

Fig. 1 shows the schematic and photos of the bionic flexible tactile sensor. Fig. 1(b) shows the image of bionic flexible tactile sensor guiding a 650-nm laser. The diameter of the MNF waist is 3.5 μm [see Fig. 1(c)]. The overall size of the sensor is 50 × 20 × 1 mm. We use a 1550-nm wavelength FP laser (THORLABS, S1FC1550PM) as the light source. A PD (THORLABS, PDA10CS-EC) is used to measure the transmitted light passing through the tactile sensor, and the PD is connected to a data acquisition card (NI, USB-4431). The data acquisition card performs analog-to-digital conversion on the signal and displays it in the terminal PC. We mixed and stirred PDMS with curing agent in the ratio of 10:1, and 0.3 mL of degassed PDMS was dropped onto a 75 × 25 mm glass slide and spread evenly over the whole slide. The PDMS was cured at 80 °C for 30 min, and the cured PDMS film was cut into 50 × 20 mm to serve as a substrate for MNF. The MNF was tapered by a standard commercial single-mode fiber (Connector type: FC/PC, core diameter: 9 μm, and cladding diameter: 125 μm, Corning Inc.) by the flame stretching method [16].

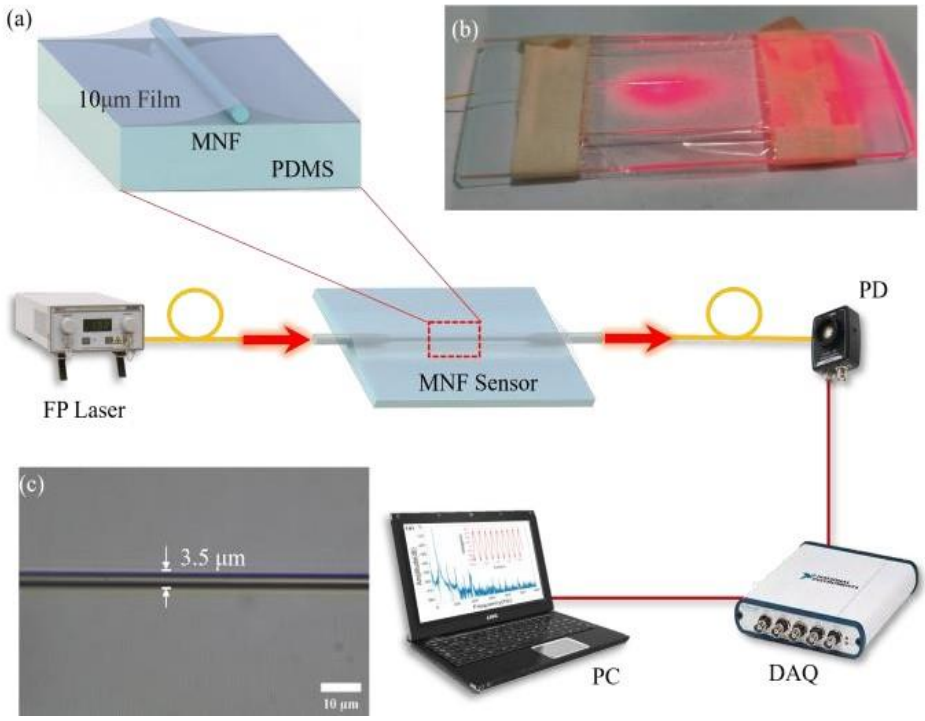

Fig. 1. (a) Schematic of the experimental setup. (b) Photograph of the bionic flexible tactile sensor guiding a 650-nm wavelength light. (c) Optical microscope image of the MNF.

First, the coating layer of the single-mode fiber was stripped 2 cm from the end face of the single-mode fiber at a location 10 cm from the end face of the single-mode fiber using fiber optic stripping pliers. Then, place the middle portion of the singlemode fiber in the middle portion of the taper puller and fix the two ends with grippers. The heating source was an alcohol lamp. The fiber should be preheated for 5 s before performing taper pulling. The speed of the taper-pulling machine should be set to 0.5 mm/s, and the stretching length should be set to 15 mm. Fuse the end face of the fiber to an FC/PC connector for connection to a laser or PD. The MNF was placed in a straight shape on a 1-mm-thick PDMS. The sensor surface was packaged with a 10-μm film (Toray Group, Lumirror, 10 μm). A ridge-shaped sensing region was formed on the surface of the PDMS after the MNF was covered by the film [see Fig. 1(a)].

B. Principle and Simulation

As an MNF is bent, a strain is induced in the fiber core and cladding (1ε), and then, the refractive index of fiber core and cladding is varied. The different strain between the cladding and core is given by [22]

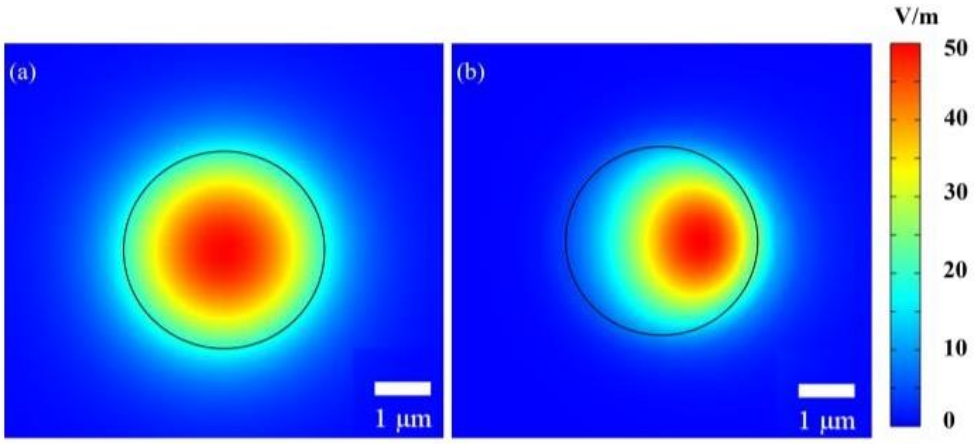

Fig. 2. Electric field intensity distribution. (a) MNF is not bent. (b) MNF bends with a radius of 10 μm.

$$\Delta\varepsilon = d/R \tag{1}$$

where d is the distance between cladding and core and R is the bending radius. Due to strain difference induced by applied pressure, the effective index difference ($1n_{\text{eff}}$) between the core and cladding of tapered fiber changes, and this change is governed by the following equation [23]:

$$\Delta n_{\text{eff}} = \Delta n_{\text{eff}}^{0} + k\Delta\varepsilon \tag{2}$$

where $1n^{0}_{\text{eff}}$ is the effective index difference without any strain or banding and k is the strain refractive index coefficient.

The phase difference 8_m between the core mode and the cladding mode after propagating through the length L of the sensor can be expressed by [24]

$$\Phi_m = 2\pi\,\Delta n_{\text{eff}}^{0} L/\lambda \tag{3}$$

where L is the length of the MNF under pressure and λ is the input wavelength.

The pressure and vibration to which the bionic flexible tactile sensor is subjected causes the PDMS to bend, deforming the waveguide structure and resulting in the transmittance change of the MNF. When the fiber is bent, the fundamental mode will partially leak into the cladding and progressively switch to the radiation mode, which results in a loss of light [25]. To demonstrate the variation of MNF under different bending deformations, numerical simulations were performed using the wave optics module (electromagnetic waves and frequency domain) of a commercial finite element simulation software. Fig. 2 shows the electric field intensity distribution of unbent and stressed bent silica microfibers with a wavelength of 1550 nm and a waist

diameter of 3.5 μm. The refractive index of the single-mode fiber is set to 1.46. The surrounding medium is set to air with a refractive index of 1. The well-confined directed modes gradually leak out and change into radiating modes as the bending radius decreases. It is obvious that a larger fractional transition of guided modes switches to radiation modes, which means higher bending loss.

III. EXPERIMENTS AND RESULTS

For tactile sensors, detecting pressure and vibration is the most basic requirement. Thanks to the ultrasensitivity of MNF, with the film-fiber-PDMS structure, the MNF is very close to the sensor surface, and vibration and pressure signals can act directly on the MNF. This approach allows the tactile sensor to be much more sensitive. When the vibration acts on the MNF, the output intensity of the laser changes. This is due to the weaker confinement in the microfiber under stress and reduced guided light transmission. We have measured the vibration signal with the tactile sensor. We use a signal generator connected to a speaker and output standard sinusoidal signals of different frequencies to the speaker (8 Ω, 0.5 W). The output voltage of the generator was set to 1 Vpp and the frequencies were set to 0.1 Hz, 0.2 Hz, 10 Hz, 50 Hz, 500 Hz, 1 kHz, and 2 kHz. We place the flat side of the speaker on the MNF flexible sensor and the speaker vibrates against the sensor.

Fig. 3(a) and (b) shows the signal and spectrum of the haptic sensor measuring a vibration of 0.1 Hz. Fig. 3(c) and (d) shows the signal and spectrum of the tactile sensor measuring the vibration at 0.2 Hz. Fig. 3(e) and (f) shows the signal and spectrum of the tactile sensor measuring 10-Hz vibration. Fig. 3(g) and (h) shows the signal and spectrum of the tactile sensor measuring a vibration of 50 Hz. Fig. 3(i) and (j) shows the signal and spectrum of the tactile sensor measuring a vibration of 500 Hz. Fig. 3(k) and (l) shows the signal and spectrum of a tactile sensor measuring a vibration of 1 kHz. Fig. 3(m) and (n) shows the signal and spectrum of the tactile sensor measuring 2-kHz vibration. The tactile sensor is able to accurately convert the vibration signal into a change in light intensity.

The detection and recognition of texture materials on the surface of contact objects is also very important for tactile sensors. Due to the use of thin film-MNF-PDMS structure to form a ridge sensing area on the sensor surface, different textures and materials across the surface of the tactile sensor can produce significantly different signals. In the experiment, we used the surface of the finger sleeve with raised points [see Fig. 4(a)] and the surface of the index finger [see Fig. 4(b)] to move across the sensor surface. We used a 1550-nm FP laser as a light source and a photodetector to measure the transmitted light intensity. An acquisition card was used to capture the signals from the photodetector with a sampling frequency of 50 kHz. Due to the different material and texture of the contact surface, the pressure and vibration frequency generated on the ridge sensing area are also different, which leads to the amplitude and frequency of the output signal. Fig. 4(c) and (d) shows the transmitted light intensity signal after normalization between 0 and 1.

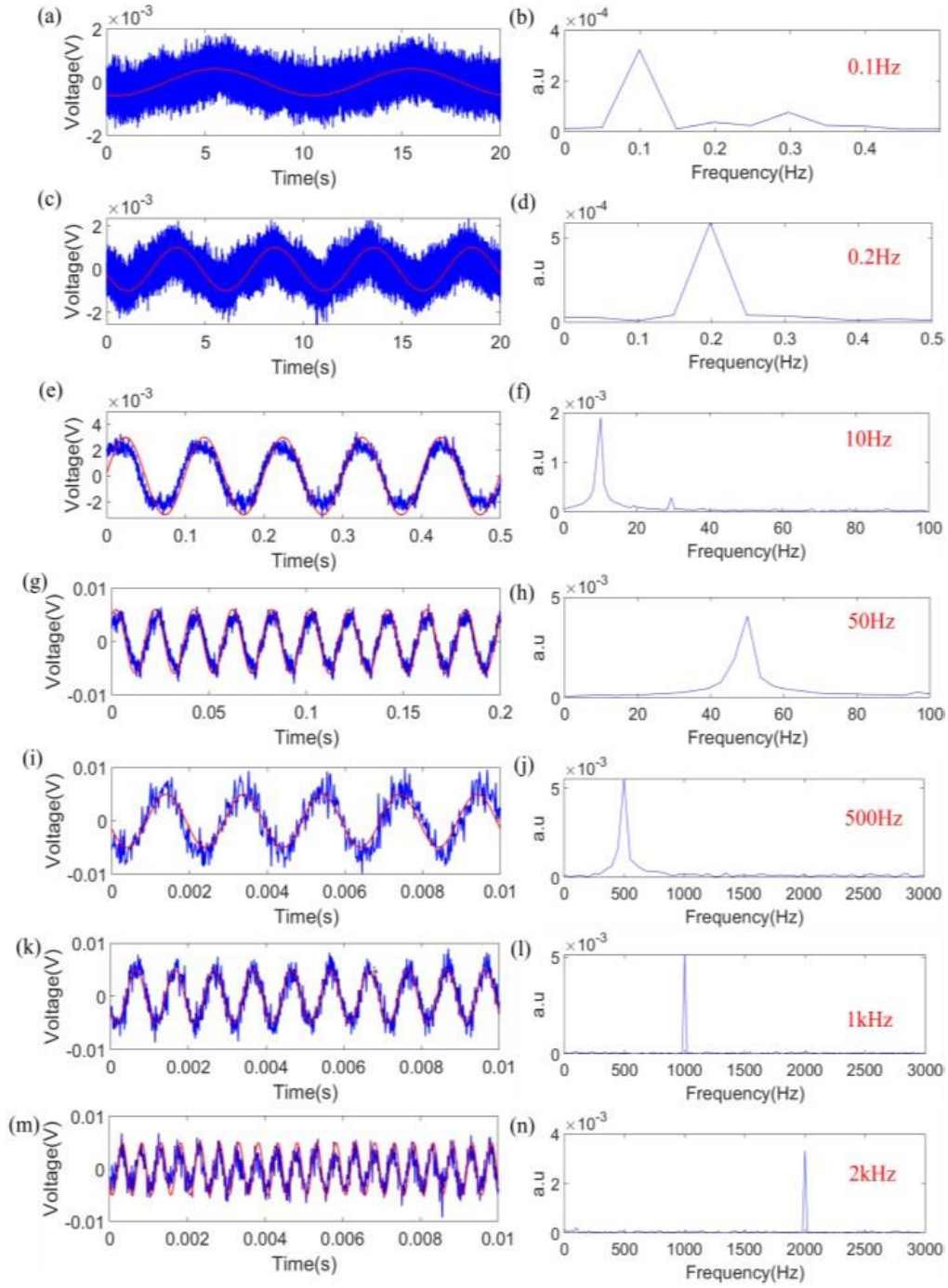

Fig. 3. Vibration signal and spectrum at frequencies of (a) and (b) 0.1 Hz, (c) and (d) 0.2 Hz, (e) and (f) 10 Hz, (g) and (h) 50 Hz, (i) and (j) 500 Hz, (k) and (l) 1 kHz, and (m) and (n) 2 kHz. The red line is the original signal.

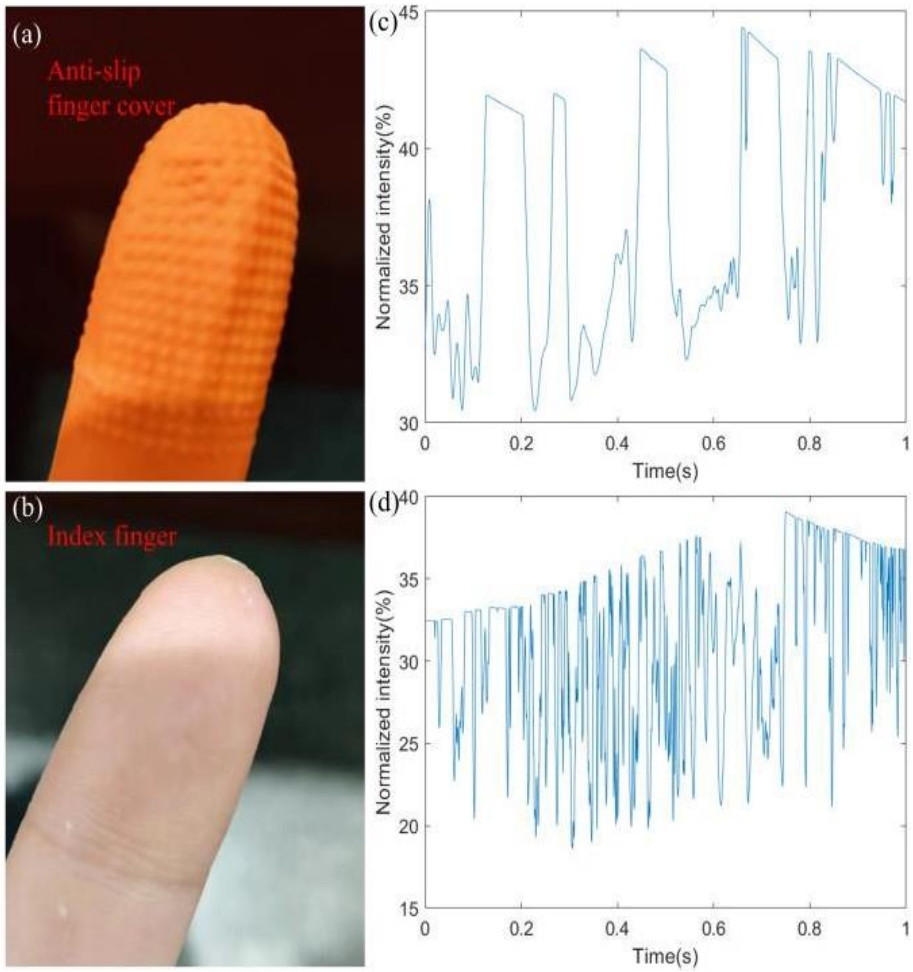

Fig. 4. (a) Antislip finger cover with bumps. (b) Surface of the index finger. (c) Signal of antislip finger cover scratching the sensor surface. (d) Signal of index finger scratching the sensor surface.

To further test the tactile sensor's recognition of the texture of the contact surface, we set the tactile sensor to test the surface with different roughness of the same material. We used different grit numbers of sandpaper and let it slide on the sensor surface for 4 s under the same pressure. A motorized slide is used to control the sliding speed. The sliding speed is 10 mm/s. We chose 50-g weights to provide the same pressure. Sandpaper was cut into 2 × 20 cm strips. The smooth transparent tape was applied to the back of the sandpaper to eliminate interference. Sandpaper with grit numbers of 320, 400, 600, 800, 1000, 1500, and 2000 CW was selected for sliding measurement. Ten sets of signals were collected for each grit number to verify the accuracy of the data measurement. We plot a curve based on the mean and standard deviation of the data. The results of signal measurement are shown in Fig. 5. The transmitted light intensity signal is normalized between 0 and 1. The black scatter is the measured data with error bars and the red curve is the fit curve based on exponential fitting. As the grit of the sandpaper increases, the roughness of the sandpaper gradually decreases.

We analyzed the results of roughness measurements with extended uncertainty, where the sources of uncertainty are uncertainty due to repeated measurements, uncertainty due to laser input and PD output, and uncertainty due to the acquisition card. The extended uncertainty of the roughness measurement is 0.7%.

Under the same pressure applied to the sandpaper, when the sandpaper slides, the surface of the sandpaper with high grit number (CW) is relatively smooth, and the surface particles

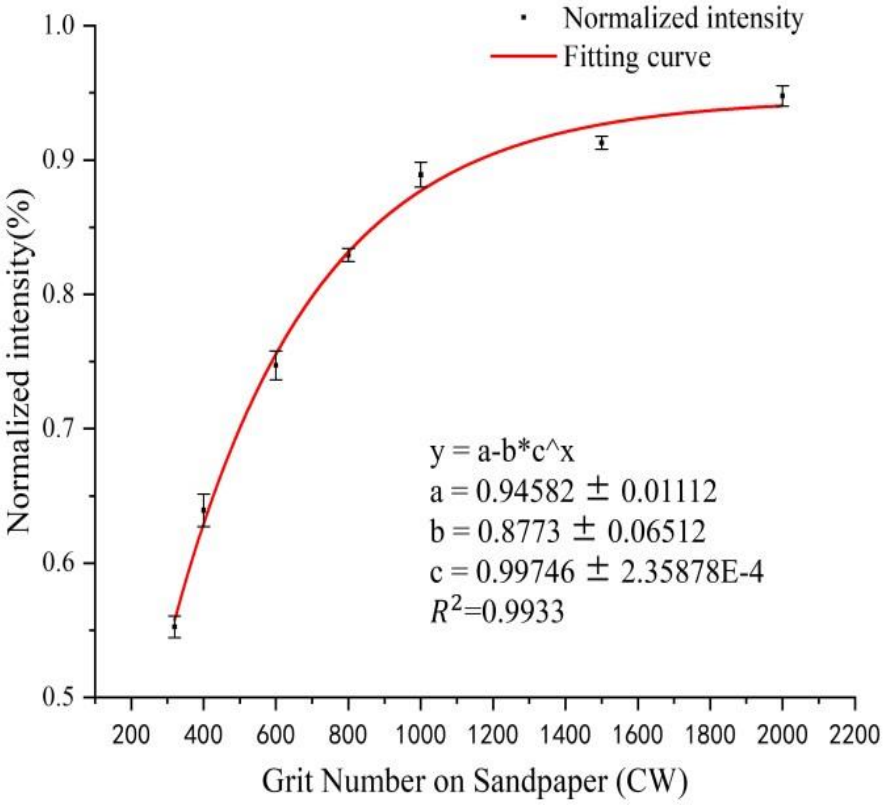

Fig. 5. Signal produced by the sliding of different grit sandpaper on the sensor.

of the sandpaper have a large area of contact with the MNF, resulting in a smaller pressure acting on the MNF and, therefore, a larger intensity of transmitted light. On the contrary, when the sandpaper grit number is small, the area of the sandpaper in contact with the MNF is smaller, and the pressure exerted on the MNF is greater, resulting in a smaller intensity of transmitted light. It is worth mentioning that the sandpaper surface particles are silicon carbide. Its Mohs hardness of 9.5 is much higher than that of silica MNF. In the same sensor slip test bell hundreds of times, the 10-μm film did not wear. It has sufficient strength to encapsulate and protect MNF. Besides, the sensor exhibits high static stability, and it can respond to various forces with little overshoots and swift transition.

It is worth mentioning that the MNF we used has a sufficiently large taper angle in the waist region so that it can simultaneously excite both the fundamental mode and the first higher order mode of the beam [26] (i.e., HE11 and HE12 modes, respectively). Both patterns are then collected through the second taper region. As an optical path difference exists between the HE11 and HE12 modes, such double tapered structure constitutes a Mach–Zehnder interferometer. The transmission spectrum is shifted because of the change in the refractive index of the MNF surface [27].

The resonant dip λ_m generated by the Mach–Zehnder interferometer between the HE11 mode and the HE12 mode can be expressed as [28]:

$$(n_1 - n_2)L = \Delta n_{\text{eff}} L = (p + 1/2)\lambda_m \quad (4)$$

$$\Delta n_{\text{eff}} = n_1 - n_2 = (\beta_1 - \beta_2) \times \frac{\lambda_m}{2\pi} \quad (5)$$

where n_1 and n_2 and β_1 and β_2 are the effective RI and propagation constants of the HE11 and HE12 modes, respectively, $1n_{\text{eff}}$ is the effective RI difference between the two modes, L represents the length of the MNF, and $m$is a positive integer.

With this principle, we measured the temperature response of the sensor. We plot a curve based on the mean and standard deviation of the data. As shown in Fig. 6(a), we used the PXie4844 from NI to measure the wavelength shift. The device uses a tunable laser and a high-precision wavelength scanning and

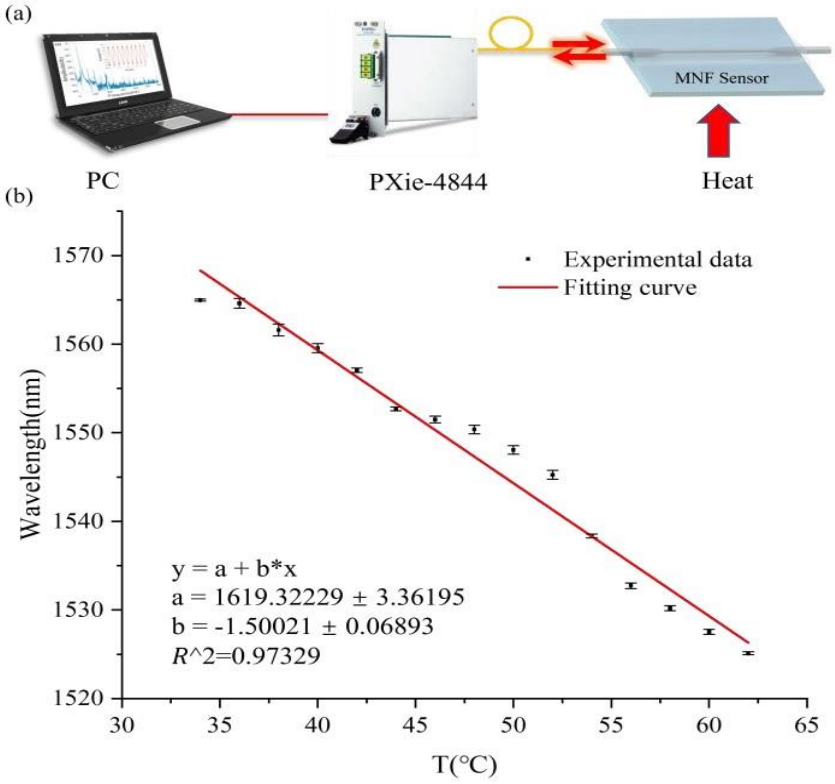

Fig. 6. (a) Schematic for temperature measurement. (b) Temperature– wavelength curve.

signal sampling synchronization system. Since the measurement is done with the return light from the fiber end face, we cut the fiber end face flat to ensure maximum reflection intensity. We use the heated bed of the 3-D printer (Anycubic I3 MEGA) to control the temperature. Temperature data were measured every 2 ◦C of change. The temperature–wavelength curve is shown in Fig. 6(b). The black scatter is the measured data with error bars and the red curve is the fit curve based on a linear fit. We performed a total of five measurements where the wavelength changed from 1565 to 1525 nm as the temperature changed from 34 ◦C to 62 ◦C. This sensor has a sensitivity of 1.43 nm/◦C. We performed an extended uncertainty analysis of the temperature measurements, where the sources of uncertainty are: uncertainty due to replicate measurements, uncertainty due to broadband light source output, and uncertainty due to spectrometer measurements. The extended uncertainty of the temperature measurement is 0.41 nm. The signals of vibration, pressure, and texture measurements are all reflected in the light intensity, so the effect of temperature changes on the signal is almost negligible.

IV. DISCUSSION

Similar to biotactile nerves [3], photonic skin is able to encode perceived pressure changes as well as vibration amplitudes into weak light signals that are converted into electrical signals by the PD. Benefiting from the encapsulation of the 10-μm film, a ridge-type ultrasensitive region is formed on the PDMS surface. Compared to MNF sensors directly embedded in PDMS, the thin film-MNF-PDMS structure improves sensitivity and response speed for measuring surface roughness and hardness of objects. We believe that the sensor has the capability of fingerprint acquisition and recognition because the width of the ridge-shaped region formed by the MNF is much smaller than the width of the fingerprint channel.

TABLE I

COMPARISON OF FIBER OPTIC SENSORS

Structure	Vibration frequency range	Temperature sensitivity
Two Peanut-Shape Structures[24]	N/A	46.8pm/℃
MNFs coupler[29]	0.5kHz~2kHz	N/A
Finger-skin-inspired flexible tactile sensor[5]	0.1Hz~1kHz	N/A
Tapered single mode fiber based acoustic sensor[23]	250Hz~2500Hz	N/A
Single optical microfiber enabled tactile sensor[18]	500Hz~1000Hz	1.2 nm/°C
Helical Microfiber Bragg Grating[30]	N/A	4.97pm/℃
Microfiber Bragg Grating[20]	N/A	0.04 nm/℃
Our work	0.1Hz~2kHz	1.43 nm/°C

We compare the work in this article with previously reported fiber optic vibration or temperature sensors. Wu et al. [24] designed a Mach–Zehnder interferometer consisting of a cascade of two peanut-shaped structures in a single-mode optical fiber and realized a temperature measurement with a sensitivity of 46.8 pm/°C. Yu et al. [29] encapsulated two incidentally coupled MNFs as in a flexible PDMS to form a highly sensitive and fast-responding strain sensor, realizing vibration measurements in the range of 0.5–2 kHz. Jiang et al. [5] reported a finger skin-inspired flexible optical sensor based on ultrafine optical fibers to achieve vibration measurements in the range of 0.1 Hz–1 kHz. Dass and Jha [23] combined a tapered optical fiber with an acrylonitrile polymer diaphragm to form an acoustic sensor, which measured vibrations in the range of 250–2500 Hz. Yao et al. [18] designed and fabricated a flexible fiber optic sensor that can simultaneously measure temperature and pressure with a temperature sensitivity of 1.2 nm/°C and a vibration measurement range of 500–1000 Hz. Liao et al. [30] presented a microfiber helical Bragg grating for refractive index measurement with a temperature measurement sensitivity of 4.97 pm/°C. Yue et al. [20] reported a flexible wearable optical sensor with a microfiber Bragg grating (μFBG) as the core sensing node and a flexible PDMS film as the sensor package with a measurement temperature sensitivity of 0.04 nm/°C. Here, we have created a comparison table, as shown in Table I.

Tactile sensing requires sensors with high enough sensitivity and large enough range. As can be seen from Table I, the thin film-MNF-PDMS structure provides our sensors with higher temperature measurement sensitivity and larger vibration measurement range.

V. CONCLUSION

In summary, we propose a novel bionic flexible tactile sensor with a thin film-MNF-PDMS structure. We use a 10-μm film to cover the MNF on PDMS for packaging. A ridge area is formed after covering the MNF. The MNF is so close to the sensor surface that vibration and pressure signals can act directly on the MNF. Such encapsulated MNF detects external stimuli in a manner similar to the sensory receptors and nerve fibers in the skin. The response of the sensor to vibration ranges from 0.1 Hz to 2 kHz. Due to the use of thin film-MNF-PDMS structure to form a ridge sensing area on the PDMS surface, different textures, and materials across the surface of the tactile sensor can produce significantly different signals. We also measured the temperature response of the sensor using a broadband light source with a spectrometer. This sensor has a sensitivity of 1.43 nm/$^{\circ}$C.

It is worth mentioning that this sensor still works well after two months of storage. The sensor exhibits high static stability, and it can respond to various forces with little overshoots and swift transition. In the same sensor slip test bell hundreds of times, the 10-μm film did not wear. It has sufficient strength to encapsulate and protect MNF. Compared to previous NMF flexible sensors, our work simplifies the fabrication process and improves sensitivity. This sensor currently uses only one MNF, and in the future, multiple MNFs can be added to increase the response area of the tactile sensor and to be able to collect multiple sets of signals at the same time. The structural and functional characteristics of this sensor are desirable in flexible bionic devices and advanced robots.

REFERENCES

[1] Y. Wu et al., "A skin-inspired tactile sensor for smart prosthetics," *Sci. Robot.*, vol. 3, no. 22, Sep. 2018, Art. no. eaat0429, doi: 10.1126/scirobotics.aat0429.

[2] J. Tang, C. Zhao, Q. Luo, Y. Chang, Z. Yang, and T. Pan, "Ultrahigh-transparency and pressure-sensitive iontronic device for tactile intelligence," *NPJ Flexible Electron.*, vol. 6, no. 1, Jun. 2022, doi: 10.1038/s41528-022-00162-y.

[3] S.-H. Woo, E. A. Lumpkin, and A. Patapoutian, "Merkel cells and neurons keep in touch," *Trends Cell Biol.*, vol. 25, no. 2, pp. 74–81, Feb. 2015, doi: 10.1016/j.tcb.2014.10.003.

[4] S.-H. Woo et al., "Piezo2 is required for merkel-cell mechanotransduction," *Nature*, vol. 509, no. 7502, pp. 622–626, May 2014, doi: 10.1038/nature13251.

[5] C. Jiang, Z. Zhang, J. Pan, Y. Wang, L. Zhang, and L. Tong, "Fingerskin-inspired flexible optical sensor for force sensing and slip detection in robotic grasping," *Adv. Mater. Technol.*, vol. 6, no. 10, Oct. 2021, Art. no. 2100285, doi: 10.1002/admt.202100285.

[6] P. Wang et al., "Smart laparoscopic grasper integrated with fiber Bragg grating based tactile sensor for real-time force feedback," *J. Biophoton.*, vol. 15, no. 5, May 2022, Art. no. e202100331, doi: 10.1002/jbio.202100331.

[7] J. Oh, S. Kim, S. Lee, S. Jeong, S. H. Ko, and J. Bae, "A liquid metal based multimodal sensor and haptic feedback device for thermal and tactile sensation generation in virtual reality," *Adv. Funct. Mater.*, vol. 31, no. 39, Sep. 2021, Art. no. 2007772, doi: 10.1002/adfm.202007772.

[8] K. Kanao et al., "Highly selective flexible tactile strain and temperature sensors against substrate bending for an artificial skin," *RSC Adv.*, vol. 5, no. 38, pp. 30170–30174, 2015, doi: 10.1039/c5ra03110a.

[9] X.Zhu,Z. Qian, X. Chen, L. Liu, C. Sheng, and W. Gu, "Electrohydrodynamics-printed silver nanoparticle flexible pressure sensors with improved gauge factor," *IEEE Sensors J.*, vol. 21, no. 5, pp. 5836–5844, Mar. 2021, doi: 10.1109/JSEN.2020.3038086.

[10] H. Zhu et al., "Self-assembled wavy optical microfiber for stretchable wearable sensor," *Adv. Opt. Mater.*, vol. 9, no. 11, Jun. 2021, Art. no. 2002206, doi: 10.1002/adom.202002206.

[11] D. Lo Presti et al., "Fiber Bragg gratings for medical applications and future challenges: A review," *IEEE Access*, vol. 8, pp. 156863–156888, 2020, doi: 10.1109/ACCESS.2020.3019138.

[12] L. Massari et al., "Functional mimicry of Ruffini receptors with fibre Bragg gratings and deep neural networks enables a bio-inspired large-area tactile-sensitive skin," *Nature Mach. Intell.*, vol. 4, no. 5, pp. 425–435, May 2022, doi: 10.1038/s42256-022-00487-3.

[13] H. Liu et al., "Optical microfibers for sensing proximity and contact in human–machine interfaces," *ACS Appl. Mater. Interfaces*, vol. 14, no. 12, pp. 14447–14454, Mar. 2022, doi: 10.1021/acsami. 1c23716.

[14] K. Xu, Y. Lu, and K. Takei, "Multifunctional skin-inspired flexible sensor systems for wearable electronics," *Adv. Mater. Technol.*, vol. 4, no. 3, Mar. 2019, doi: 10.1002/admt.201800628.

[15] W. Yan et al., "Single fibre enables acoustic fabrics via nanometre-scale vibrations," *Nature*, vol. 603, no. 7902, pp. 616–623, Mar. 2022, doi: 10.1038/s41586-022-04476-9.

[16] Y. Kang et al., "Fabrication methods and high-precision diameter control techniques of optical micro-/nanofibers," *SCIENTIA SINICA Phys., Mechanica Astronomica*, vol. 50, no. 8, Aug. 2020, Art. no. 084212, doi: 10.1360/sspma-2020-0027.

[17] H. Liang et al., "Wearable and multifunctional self-mixing microfiber sensor for human health monitoring," *IEEE Sensors J.*, vol. 23, no. 3, pp. 2122–2127, Feb. 2023, doi: 10.1109/JSEN.2022.3225196.

[18] N. Yao et al., "Single optical microfiber enabled tactile sensor for simultaneous temperature and pressure measurement," *Photon. Res.*, vol. 10, no. 9, p. 2040, 2022, doi: 10.1364/PRJ.461182.

[19] L. Zhang et al., "Ultrasensitive skin-like wearable optical sensors based on glass micro/nanofibers," *Opto-Electron. Adv.*, vol. 3, no. 3, pp. 19002201–19002207, 2020, doi: 10.29026/oea.2020. 190022.

[20] X. Yue et al., "Flexible wearable optical sensor based on optical microfiber Bragg grating," *J. Lightw. Technol.*, vol. 41, no. 6, pp. 1858–1864, Dec. 6, 2023, doi: 10.1109/jlt.2022.
3227186.

[21] B.-O. Guan, Y. Ran, F.-R. Feng, and L. Jin, "Formation and applications of the secondary fiber Bragg grating," *Sensors*, vol. 17, no. 2, p. 398, Feb. 2017, doi: 10.3390/s17020398.

[22] H. Gong, X. Yang, K. Ni, C.-L. Zhao, and X. Dong, "An optical fiber curvature sensor based on two peanut-shape structures modal interferometer," *IEEE Photon. Technol. Lett.*, vol. 26, no. 1, pp. 22–24, Nov. 5, 2014, doi: 10.1109/LPT.2013.2288978.

[23] S. Dass and R. Jha, "Tapered fiber attached nitrile diaphragm-based acoustic sensor," *J. Lightw. Technol.*, vol. 35, no. 24, pp. 5411–5417, Dec. 15, 2017, doi: 10.1109/JLT.2017.2776519.

[24] D. Wu, T. Zhu, K. S. Chiang, and M. Deng, "All single-mode fiber Mach–Zehnder interferometer based on two peanut-shape structures," *J. Lightw. Technol.*, vol. 30, no. 5, pp. 805–810, Jan. 2, 2012, doi:
10.1109/JLT.2011.2182498.

[25] Z. Zhang et al., "A multifunctional airflow sensor enabled by optical micro/nanofiber," *Adv. Fiber Mater.*, vol. 3, no. 6, pp. 359–367, Dec. 2021, doi: 10.1007/s42765-021-00097-5.

[26] B.-O. Guan and Y. Huang, "Interface sensitized optical microfiber biosensors," *J. Lightw. Technol.*, vol. 37, no. 11, pp. 2616–2622, Dec. 23, 2019, doi: 10.1109/JLT.2018.2889324.

[27] Y. Huang, P. Chen, H. Liang, A. Xiao, S. Zeng, and B.-O. Guan, "Nucleic acid hybridization on a plasmonic nanointerface of optical microfiber enables ultrahigh-sensitive detection and potential photothermal therapy," *Biosensors Bioelectron.*, vol. 156, May 2020, Art. no. 112147, doi: 10.1016/j.bios.2020.112147.

[28] H. Luo et al., "Refractive index sensitivity characteristics near the dispersion turning point of the multimode microfiber-based Mach–Zehnder interferometer," *Opt. Lett.*, vol. 40, no. 21, pp. 5042–5045, 2015, doi: 10.1364/OL.40.005042.

[29] W. Yu et al., "Highly sensitive and fast response strain sensor based on evanescently coupled micro/nanofibers," *Opto-Electron. Adv.*, vol. 5, no. 9, p. 210101, 2022, doi: 10.29026/oea.2022.210101.

[30] C.Liao, K. Yang, J. Wang, Z. Bai, Z.Gan, and Y. Wang, "Helical microfiber Bragg grating printed by femtosecond laser for refractive index sensing," *IEEE Photon. Technol. Lett.*, vol. 31, no. 12, pp. 971–974, Apr. 23, 2019, doi: 10.1109/LPT.2019.2912634.